Photochemistry and Photobiology, 2006, 82: 123–131

# Control of Chirality by Cations in Confined Spaces: Photooxidation of Enecarbamates Inside Zeolite Supercages†

**J. Sivaguru[1], Hideaki Saito[1,2], Marissa R. Solomon[1], Lakshmi S. Kaanumalle[3], Thomas Poon[4], Steffen Jockusch[1], Waldemar Adam[5], V. Ramamurthy[3], Yoshihisa Inoue[2] and Nicholas J. Turro*[1]**

[1]The Department of Chemistry and the Department of Chemical Engineering, Columbia University, New York, NY
[2]The Department of Molecular Chemistry, Osaka University, Suita, Japan and The Entropy Control Project, ICORP, JST, Toyonaka, Japan
[3]Department of Chemistry, University of Miami, Coral Gables, FL
[4]Joint Science Department, W.M. Keck Science Center, Claremont McKenna, Pitzer, and Scripps Colleges, Claremont, CA
[5]Institute für Organische Chemie, Universität Würzburg, Würzburg, Germany, and the Department of Chemistry, University of Puerto Rico, Rio Piedras, PR

**Received 15 June 2005; accepted 20 July 2005; published online 02 August 2005 DOI: 10.1562/2005-06-15-RA-573**

## ABSTRACT

**On photooxygenation of the optically active *Z/E* enecarbamates 1 (X = *i*-Pr) and 2 (X = Me) equipped with the oxazolidinone chiral auxiliary in methylene-blue (MB)-incorporated, alkali-metal (M = Li, Na, K, Cs, Rb), exchanged Y-type zeolites (MY-MB), oxidative cleavage of the alkenyl functionality releases the enantiomerically enriched methyldesoxybenzoin (MDB) product. The extent (%ee) and/or the sense (*R* or *S*) of the stereoselectivity in the formation of the MDB product depends on the choice of the alkyl substiuent (*i*-Pr or Me) at the *C*-4 position of the oxazolidinone chiral auxiliary, the *Z/E* configuration of the alkene functionality in the enecarbamates, and the type of alkali metal in the zeolite. Most significantly—the highlight of this study—is the reversed sense (*R* or *S*) in the stereoselection when the photooxygenation is run in $CDCl_3$ solution *versus* inside the MY-MB zeolite. As a mechanistic rationale for this novel stereochemical behavior, we propose the combined action of spatial confinement and metal-ion coordination (assessed by density-functional calculations) of the substrate within the zeolite supercage, both of which greatly reduce the freedom of the substrate and entropically manipulate the stereochemical outcome.**

## INTRODUCTION

The achievement of high enantioselectivity in photochemical reactions (1–4) has fascinated photochemists for decades (5–7). For effective asymmetric induction, the spatial requirements of the excited states or reactive intermediates (or both) must be manipulated within their short lifetimes to imprint stereocontrol in the product. For this purpose, chirally modified zeolites have been shown to be beneficial in achieving high stereoselectivity in photoreactions (3,8,9). In the present work we utilize the spatial confinement offered by the dye-exchanged Y zeolites to impose stereocontrol in the photooxidative cleavage of enecarbamates equipped with the oxazolidinone chiral auxiliary for asymmetric induction in the resulting product (10–12).

Faujasite-type Y zeolites have the composition $M_{56}$ $(AlO_2)_{56}$ $(SiO_2)_{136}$ $253H_2O$ of the unit cell, for which M is a monovalent metal ion (13–15). The cage structure is constructed of openings containing 4- and 6-membered rings of $[SiO_4]^{4-}$ and $[AlO_4]^{5-}$ polyhedra, the so-called *sodalite* cages. While these sodalite cages are too small to accommodate organic molecules, they tetrahedrally arrange to form a three-dimensional network of larger void spaces, which are known as the *supercages* (see Fig. 1).

Typically there are eight supercages per unit cell in the case of Faujasite-type Y zeolite, with a void space of ~14 Å in diameter. This supcercage is interconnected to four other supercages by tetrahedrally disposed 12-membered-ring windows of ~8 Å in diameter (see Fig. 1) to form a three-dimensional network. An organic guest molecule may diffuse into the supercage through the channels and cages by way of the 12-membered-ring windows.

One of the main features of Faujasite-type Y zeolites is the charge-compensating alkali/alkaline-earth metal ions (16) that occupy the three types of positions I, II and III (NaY with an Si/Al ratio of 2.4 has 55 metal ions per unit cell) (13–18). Type I metal ions are generally too deeply buried within the sodalite cages to interact with the caged guest molecule; thus, only Type II and Type III metal ions are readily accessible. The metal ions are hydrated under ambient condition and the water molecules are generally located in the cages, cavities and channels of the zeolites. When the water is removed at elevated temperature, organic guest

* To whom correspondence should be addressed: 3000 Broadway, Mail Code 3119, New York, NY 10027, USA. Fax: 212-932-1289; e-mail: njt3@columbia.edu

† This paper is part of a special issue dedicated to Professor J. C. (Tito) Scaiano on the occasion of his 60th birthday.

*Abbreviations:* ee, enantioselectivity; GC, gas chromatography; MB, methylene blue sensitizer; MDB, methyldesoxybenzoin; MY, alkali-metal-ion-exchanged Faujasite type Y-zeolites; NMR, nuclear magnetic resonance; RB3LYP, restricted Becke three-parameter exchange functional of Lee-Yang-Parr; $^1O_2$, singlet oxygen.

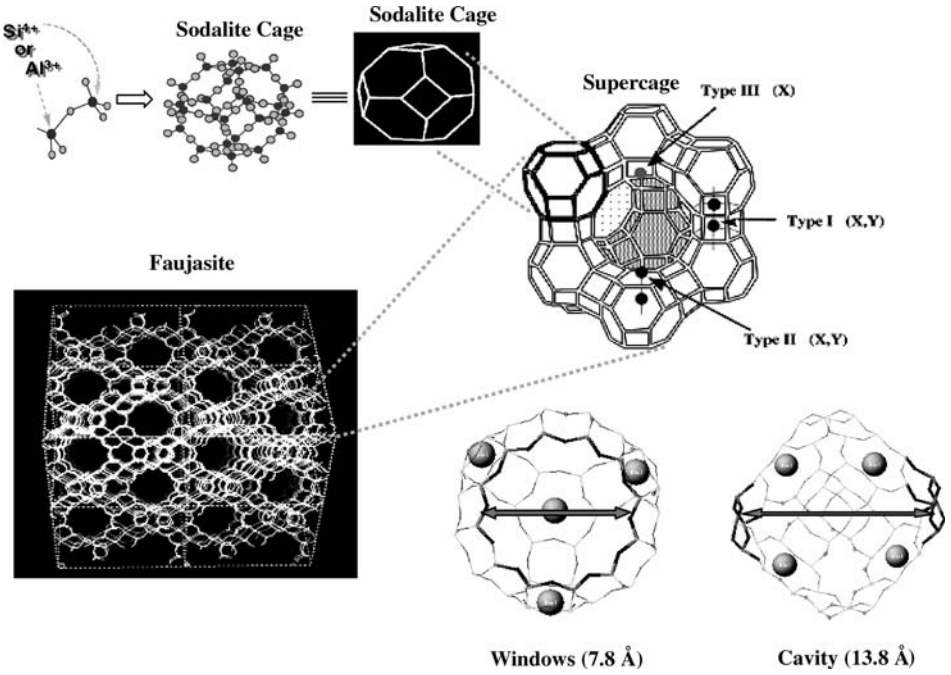


**Figure 1.** Architecture of Faujasite Y-zeolite, location of the cations and the size of the cavity and the window.

molecules may be caged within these voids and the metal ions abandon their original position to bind with the organic occupant (17–23). The binding interaction depends on the charge density of the metal ion (*i.e.* the higher its charge density, the stronger the binding). Furthermore, these metal ions may be readily exchanged for cationic organic dyes such as methylene blue (MB) (24). The latter is an efficient singlet-oxygen sensitizer and, expectedly, MB-exchanged alkali-meta-ion-exchanged Faujasite-type Y-zeolites (MY) (MY-MB) (24) have been employed effectively in the photooxygenation of alkenes within the confined space of the zeolite (25–30), as shall be demonstrated in this article.

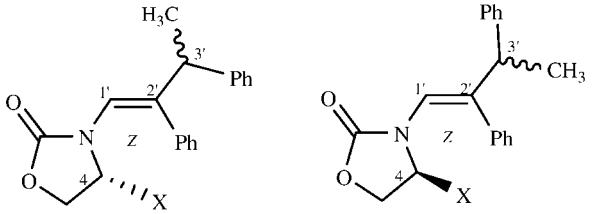


X = *iPr*- *Z(R)*-**1** : *Z*-4*R(iPr)*,3'(*R/S*) *Z(S)*-**1** : *Z*-4*S(iPr)*,3'(*R/S*)

X = *Me*- *Z(R)*-**2** : *Z*-4*R(Me)*,3'(*R/S*) *Z(S)*-**2** : *Z*-4*S(Me)*,3'(*R/S*)

X = *H*- *Z*-**3** : *Z*-4(*H*),3'(*R/S*)

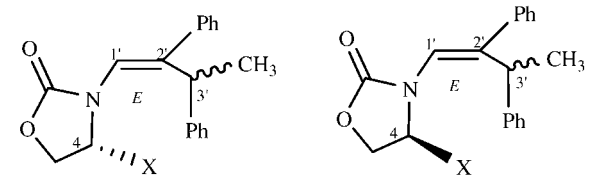


X = *iPr*- *E(R)*-**1** : *E*-4*R(iPr)*,3'(*R/S*) *E(S)*-**1** : *E*-4*S(iPr)*,3'(*R/S*)

X = *Me*- *E(R)*-**2** : *E*-4*R(Me)*,3'(*R/S*) *E(S)*-**2** : *E*-4*S(Me)*,3'(*R/S*)

**Figure 2.** Oxazolidinone-functionalized *E* and *Z* enecarbamates employed in this study.

The alkenes, which have been photooxygenated with singlet oxygen (31–34) herein are the chiral oxazolidinone-substituted enecarbamates (10–12,35,36) in Fig. 2. These constitute versatile and informative substrates for the study of conformational, electronic, stereoelectronic and steric effects on the stereoselectivity in the oxidation of the alkene functionality (10–12,35,36). For example, an enantiomeric excess (ee) as high as 97% has been achieved in the methyldesoxybenzoin (MDB) product during the photooxygenation of the *E*(*R*)-**1** enecarbamate in methanol-$d_4$ at –70°C (36). This photooxidation in solution was shown to depend on the configuration of the double bond; the *E* isomer gave consistently a higher stereoselectivity than the corresponding *Z* isomer. Even at very low temperatures, only a modest enantioselectivity (about 25%) was obtained in the MDB product for the readily synthesized *Z* isomer (10–12). To ascertain asymmetric induction for the *Z* isomer, we turned to the Y zeolites (35), which are known to enhance the efficacy of enantiocontrol by the chiral auxiliary in photoreactions through the spatial confinement imposed in the zeolite supercage (8,37,38).

To take advantage of such zeolite chemistry in facilitating asymmetric induction, the photooxygenation of the oxazolidinone-functionalized *E* and *Z* enecarbamates (50:50 diastereomeric mixtures of the *R*/*S* isomers at the *C*-3′ position in the alkene moiety were used) shown in Fig. 2 have been investigated in this work. MB-exchanged Y zeolites (MY-MB) prepared by cation exchange (25,39) were utilized for the photooxidative cleavage of the alkenyl functionality in these chiral enecarbamates, to produce the enantiomerically enriched MDB (35). No enantiocontrol would afford a racemic MDB, whereas perfect enantiocontrol would generate one of its enantiomers exclusively. The extent and the sense in the enantioselectivity was to be probed by varying the alkyl substituent (see Fig. 2) and the configuration at the *C*-4 position of the oxazolidinone chiral auxiliary,

**Table 1.** Enantioselective photooxygenation of 4-isopropyloxazolidinone-functionalized enecarbamates **1** in chloroform solution and inside NaY-MB zeolite.

| Medium* | Enecarbamate† | hυ (min) | Conversion‡ (%) | Mb‡§ (%) | MDB‖ (%ee) |
|---|---|---|---|---|---|
| $CDCl_3$ | *Z*(*R*)-**1** | 20 | 49 | 94 | 27 (*R*) |
| $CDCl_3$ | *Z*(*S*)-**1** | 20 | 47 | 96 | 11 (*S*) |
| NaY-MB | *Z*(*R*)-**1** | 10 | 49 | 89 | 74 (*S*) |
| NaY-MB | *Z*(*S*)-**1** | 10 | 41 | 86 | 80 (*R*) |
| $CDCl_3$ | *E*(*R*)-**1** | 20 | 47 | 92 | 55 (*R*) |
| $CDCl_3$ | *E*(*S*)-**1** | 20 | 50 | 95 | 40 (*S*) |
| NaY-MB | *E*(*R*)-**1** | 10 | 33 | 71 | 63 (*R*) |
| NaY-MB | *E*(*S*)-**1** | 10 | 31 | 75 | 62 (*S*) |

* Entries in rows 3, 4, 7 and 8 are methylene-blue-exchanged MY zeolite, prepared as reported in (25); the methylene blue was loaded as one molecule per 150 supercages.
† The enecarbamates were loaded as a 50:50 mixture of 3′(*R*/*S*) diastereomers, one molecule per 15 supercages.
‡ The conversion and mass balance (Mb) were determined by using 4,4′-di-*tert*-butylbiphenyl as calibration standard on an achiral stationary phase; values are averages of three runs within ±5% error of the stated values.
§ The mass balance (Mb) without irradiation (thermal control) in NaY-MB is 90% for *Z*(*R*)-**1**/*Z*(*S*)-**1** and 85% for *E*(*R*)-**1**/*E*(*S*)-**1** (41).
‖ Analyzed by GC on a chiral stationary phase; values are within ±5% error of the stated values.

by examining the influence of the *E*/*Z* geometry of the alkene functionality, and by changing the type of alkali metal ion in the MB-exchanged MY-MB zeolite; the zeolite data were to be compared with the photooxygenation in $CDCl_3$ solution.

The results of this extensive investigation are reported herewith. Evidently, the spatial confinement offered by zeolites constitutes a promising stereochemical methodology to effect the enantioselective photooxidative cleavage of chiral alkenes.

## MATERIALS AND METHODS

*Materials.* Zeolite Y (NaY; CBV-100) from Zeolyst (Valley Forge, PA) was used as purchased. All solvents (Aldrich, St. Louis, MO; Fisher, Fairlawn, NJ; Acros Organics, Geel, Belgium) were used as purchased. Deuterated solvents were acquired from Cambridge Isotope Labs and used as received.

*General procedure for synthesis of the E enecarbamates.* A 0.15 mmol sample of the *Z* enecarbamate (~50:50 epimeric mixture; see Fig. 2) was dissolved in 20 mL of $CH_2Cl_2$ and placed into a quartz test tube, fitted with a septum, gas delivery needle and vent needle (10–12,35,36). The solution was purged for 20 min with dry $N_2$ gas and then irradiated at 254 nm in a Rayonet photochemical (Hamden, CT) reactor for 20–30 min under a positive $N_2$ pressure. Gas chromatography (GC) analysis of the photolysate showed that the photostationary state (*Z*:*E* = 52:48) was reached after 20 min. The solvent was removed at ~25°C and 0.5 torr on a rotatory evaporator, the residue loaded onto a 2 mm thick preparative thin-layer chromatography plate (EMD silica gel 60F), and eluted with a 2:1 mixture of hexane/methyl *tert*-butyl ether. The faster-running fraction was extracted with a 50/50 mixture of $CH_2Cl_2$/EtOAc to recover the starting material (50/50 epimeric mixture of *Z* enecarbamate). The slower-running fraction was extracted with 50/50 $CH_2Cl_2$/EtOAc to give 0.07 mmol of the *E* enecarbamate (~50:50 epimeric pair). All the *E*/*Z* enecarbamates used in this work have been reported in the literature (10–12,35,36).

*Instrumentation.* GC analyses were performed on a Varian 3900 gas chromatograph (Palo Alto, CA) equipped with an autosampler. A Varian Factor-4 VG-1 ms column (l = 25 m, id = 0.25 mm, df = 0.25 μm) was employed for the separation on the achiral stationary phase, with a program of 50°C for 4 min, raised to 225°C at 10°C/min, and kept at 225°C for 10 min. A Varian CP-Chirasil-DEX CB (l = 25 m, id = 0.25 mm, df = 0.25 μm) was used for the separations on the chiral stationary phase, with a program of 135°C for 70 min, raised to 200°C at 15°C/min, and kept at 200°C for 30 min. The $^1$H-nuclear magnetic resonance (NMR) spectra were recorded on a 400 MHz BRUKER (Billerica, MA) spectrometer.

**Table 2.** Time dependence of the enantioselectivity in the photooxygenation of the *Z*(*R*)-**1** isomer inside NaY-MB*.

| Enecarbamate | hυ (min) | Conversion† (%) | Mb† (%) | MDB‡ (%ee) |
|---|---|---|---|---|
| *Z*(*R*)-**1** | 5 | 38 | 91 | 77 (*S*) |
| *Z*(*R*)-**1** | 10 | 49 | 87 | 74 (*S*) |
| *Z*(*R*)-**1** | 15 | ND§ | 65 | 75 (*S*) |
| *Z*(*R*)-**1** | 20 | ND§ | 55 | 78 (*S*) |
| *Z*(*R*)-**1** | 25 | ND§ | 50 | 71 (*S*) |
| *Z*(*R*)-**1** | 30 | ND§ | 58 | 80 (*S*) |

* The methylene blue was loaded in NaY as one molecule per 150 supercages, prepared as reported in (25). The loading of the substrate *Z*(*R*)-**1** [50:50 3′(*R*/*S*) epimer] was one molecule per 15 supercages.
† The conversion and mass balance (Mb) were determined by using 4,4′-di-*tert*-butylbiphenyl as calibration standard on an achiral stationary phase; values are averages of three runs within ±5% error of the stated values.
‡ Analyzed by GC on a chiral stationary phase; values are within ±5% error of the stated values.
§ Conversion not determined.

*Photooxygenation of Z/E enecarbamates in chloroform-d.* A 0.7 mL aliquot of the enecarbamate (see Fig. 2) and MB in $CDCl_3$ (enecarbamate $3.0 \times 10^{-3}$ *M*, MB $3.7 \times 10^{-4}$ *M*) was placed into the NMR tube, sealed with a rubber septum and fitted with a gas delivery needle and a vent needle. Dry $O_2$ gas was purged through the sample for 20 min, while irradiating with a 300 W halogen lamp (Holbrook, NY) equipped with a <500 nm cutoff filter. After irradiation, the samples were submitted to $^1$H-NMR spectroscopy to determine the conversion (conversion was kept below 50%). GC analysis on an achiral stationary phase afforded the mass balance (based on unreacted enecarbamate and formed MDB product) and the conversion (based on unreacted enecarbamate), by using 4,4′-di-*tert*-butylbiphenyl as calibration standard. GC analysis on a chiral stationary phase gave the enantioselectivity (%ee) of the MDB product.

*Photooxygenation of the Z/E enecarbamates inside MB-exchanged MY-zeolite.* The zeolite (300 mg) was loaded with the dye, (25) dried at 60°C and 0.1 torr for 8 h and transferred to a test tube, which contained 12 mL of isooctane or hexane. A 9.0 μmol aliquot of the enecarbamate (see Fig. 2) in 0.2 mL of methylene chloride and 1 mL isooctane or hexane was added and the test tube was sealed with a rubber septum. The dye-zeolite slurry was purged with dry $N_2$ gas for 15 min and stirred magnetically in an oil bath for 5–6 h at 70°C in isooctane or 55–60°C in hexane. After cooling to room temperature (~25°C), the test tube was fitted with a gas delivery needle and a gas vent. Dry $O_2$ was purged through the sample for 20 min, while irradiating with a 300 W halogen lamp (a <500 nm cutoff filter was used) under magnetic stirring and continuous purging of $O_2$ gas for the required time (given in Tables 1–4). The suspended zeolite was then

**Table 3.** Enantioselective photooxygenation of 4-isopropyloxazolidinone-functionalized enecarbamates inside LiY–MB zeolite.

| Medium* | Enecarbamate† | MDB‡ (% ee) |
|---|---|---|
| LiY-MB | *Z*(*R*)-**1** | 33 (*S*) |
| LiY-MB | *Z*(*S*)-**1** | 39 (*R*) |
| LiY-MB | *E*(*R*)-**1** | 31 (*R*) |
| LiY-MB | *E*(*S*)-**1** | 36 (*S*) |

* Methylene-blue-exchanged LiY zeolite (LiY-MB), prepared as reported in (25); the methylene blue was loaded as one molecule per 150 supercages.
† The enecarbamates were loaded as a 50:50 mixture of 3′(*R*/*S*) diastereomers, one molecule per 15 supercages; all irradiation were carried out for 10 min.
‡ Values are averages of three runs, the error is within ±5% of the stated values.

**Table 4.** Confinement effects on the enantioselectivity caused by the cations of the MB-exchanged zeolites in the photooxygenation of 4-methyloxazolidinone-functionalized *Z*/*E* enecarbamates **2**.

| Medium* | Free volume† (Å$^3$) | MDB‡ (% ee) | | | |
|---|---|---|---|---|---|
| | | *Z*(*R*)-**2** | *Z*(*S*)-**2** | *E*(*R*)-**2** | *E*(*S*)-**2** |
| LiY-MB | 843 | 5 (*S*) | 3 (*R*) | 0 | 0 |
| NaY-MB | 827 | 16 (*S*) | 6 (*R*) | 5 (*R*) | 3 (*S*) |
| KY-MB | 807 | 31 (*S*) | 29 (*R*) | 17 (*R*) | 6 (*S*) |
| RbY-MB | 796 | 17 (*S*) | 12 (*R*) | 43 (*R*) | 46 (*S*) |
| CsY-MB | 781 | 10 (*S*) | 6 (*R*) | 10 (*R*) | 12 (*S*) |

* Methylene-blue-exchanged zeolite (MY-MB), prepared as reported in (25); the methylene blue was loaded as one molecule per 150 supercages; the enecarbamates were loaded as a 50:50 mixture of 3′(*R*/*S*) diastereomers, one molecule per 15 supercages; the irradiations were carried out for 10 min.
† Values taken from (16).
‡ Analyzed by GC on a chiral stationary phase; values are within ±5% error of the stated value.

removed by filtration and the filtrate (isooctane or hexane) was checked for the presence of unreacted enecarbamate (no enecarbamate was observed in the filtrate). The zeolite residue was transferred to a test tube and the contained organic material extracted by stirring magnetically with 12 mL of acetonitrile in an oil bath at 70°C for 8 h. The acetonitrile supernatant was removed by filtration and the filtrate transferred to a 100 mL round-bottomed flask. The zeolite residue was further subjected to Soxhlet extraction overnight, with acetonitrile as solvent to assure complete extraction of the enecarbamate and the MDB product. The Soxhlet extract was combined with the acetonitrile filtrate and concentrated on a rotatory evaporator at 0.5 torr and 45°C. The residue was subjected to GC analysis on an achiral stationary phase to obtain the mass balance (based on unreacted enecarbamate and formed MDB product) and the conversion (based on unreacted enecarbamate), with 4,4′-di-*tert*-butylbiphenyl as the calibration standard. GC analysis of the residue on a chiral stationary phase gave the enantioselectivity (%ee) of the MDB product.

*Computations*. All computations were performed using the Gaussian 98 Revision A.11 (40) package at restricted-B3LYP (RB3LYP) level with a 6-31G(d) basis set (the coordinates of the optimized geometry in will be available upon request from the authors).

## RESULTS

The photooxidative cleavage of the 4-isopropyloxazolidinone-functionalized enecarbamates **1**, carried out within MB-exchanged NaY zeolite (NaY-MB), is shown in Scheme 1. The enantioselectivity in the MDB product as a function of the alkene geometry of the enecarbamates **1** is given in Table 1.

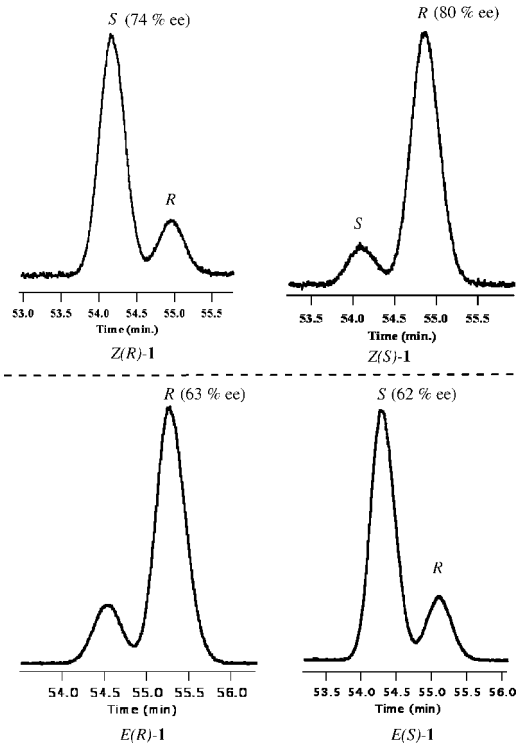


**Figure 3.** GC traces of the MDB product in the photooxygenation of the 4-isopropyloxazolidinone-functionalized *Z* (top) and *E* (bottom) enecarbamate **1** within the NaY-MB zeolite.

Compared to the photooxygenation of the *Z*(*R*)-**1** or *Z*(*S*)-**1** enecarbamates in $CDCl_3$ solution (36) (Table 1, entries 1 and 2; ee values up to 29%), much higher ee values are observed inside NaY-MB zeolite (Table 1, entries 3 and 4; up to 80%; see also Fig. 3). In contrast, the corresponding *E*(*R*)-**1** or *E*(*S*)-**1** isomers gave comparable ee values both in $CDCl_3$ solution (Table 1, entries 5 and 6; up to 55%) and inside NaY-MB zeolite (Table 1, entries 7 and 8; up to 63%; see also Fig. 3).

A closer examination of the results in Table 1 reveals for the photooxygenation inside the NaY-MB zeolite that the absolute configuration of the MDB product depends on the alkene geometry of the enecarbamate: For the *Z*(*S*)-**1** isomer, the *R*-MDB product is favored with an ee value of 80% (Table 1, entry 4; see Fig. 3), whereas for the corresponding *E*(*S*)-**1** isomer, the *S*-MDB product is preferred with an ee value of 62% (Table 1, entry 8; see Fig. 3) (35).

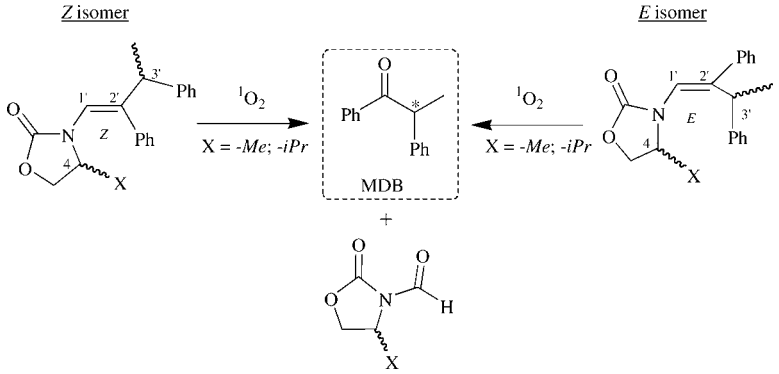


**Scheme 1.** Photooxidative cleavage of the E and Z enecarbamate to produce MDB product.

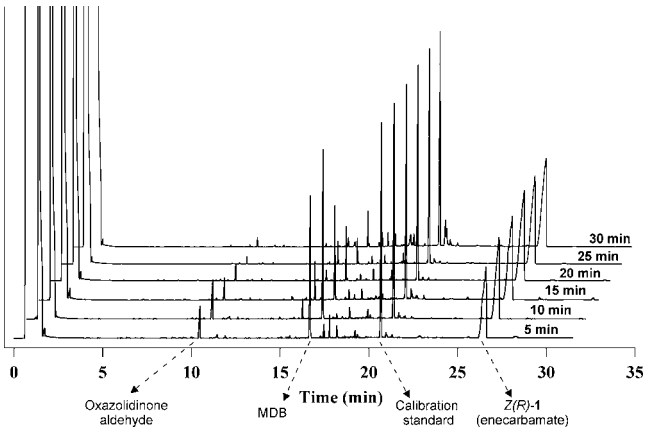


**Figure 4.** Successive GC traces (achiral stationary phase) for the photooxygenation of *Z*(*R*)-**1** inside NaY-MB at 5 min time intervals.

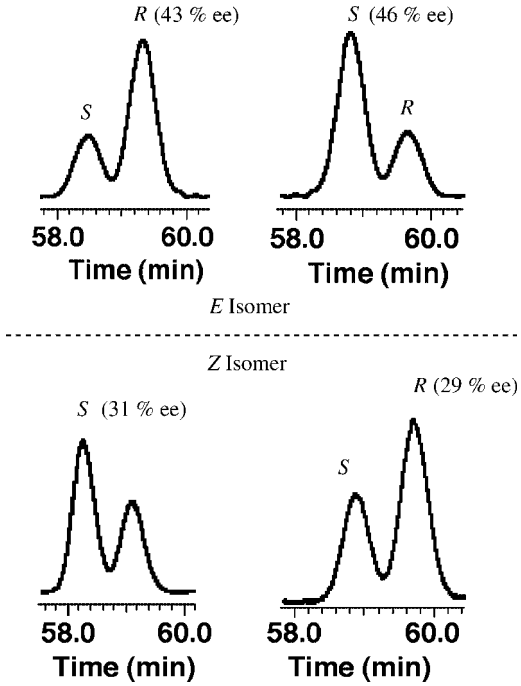


**Figure 5.** GC traces of the MDB product in the photooxygenation of the 4-methyloxazolidinone-functionalized enecarbamates **2** inside RbY (top) and KY (bottom) zeolites; *E*(*R*)-**2** (left) and *E*(*S*)-**2** (right) at the top, *Z*(*R*)-**2** (left) and *Z*(*S*)-**2** (right) at the bottom.

To examine the enantioselectivity in the MDB product as a function of enecarbamate conversion, a time-dependent study of the *Z*(*R*)-**1** photooxygenation was conducted inside the NaY-MB zeolite. The results are given in Table 2 (Fig. 4), which demonstrate that the irradiation time does not affect the enantioselectivity in the formation of the MDB product. The ee values range from 71% to 80% during the 30 min irradiation; however, the mass balance decreased considerably upon prolonged irradiation; namely, it dropped from ~90% (Table 2, entry 1) for the 5 min irradiation to ~55% (Table 2, entry 6) for 30 min. GC analysis disclosed that the MDB was consumed on prolonged irradiation due to side reactions. As a control, the caged enecarbamates were subjected to the photooxygenation conditions but without irradiation to assess the persistence of the enecarbamates within the zeolite in the dark (41). Mass balances of about ~90% were observed for the 4-isopropyloxazolidinone-functionalized enecarbamate **1** and no MDB product was detected under these conditions. Thus, the enecarbamates persist within the zeolite in the dark, which confirms that the MDB product is formed only during photooxygenation.

To determine the influence of the exchanged cation in the zeolite (8) the photooxygenation of the 4-isopropyloxazolidinone-functionalized *E*/*Z* enecarbamates (Scheme 1) was carried out in MB-exchanged LiY zeolite (LiY-MB). The %ee values of the MDB product are collected in Table 3, which exhibits that the same enantiomer of the MDB product was enhanced within both zeolites LiY-MB (Table 3) and NaY-MB (Table 1) for a given enecarbamate **1**, but the enantioselectivity in the MDB product is considerably lower for the LiY-MB zeolite. For example, the %ee value of *Z*(*S*)-**1** is 80% *R*-MDB within NaY-MB (Table 1, entry 4) compared to only 39% *R*-MDB within LiY-MB (Table 3, entry 2). Also the photooxygenation of the 4-isopropyloxazolidinone-functionalized enecarbamate **1** was attempted within MB-exchanged KY, RbY and CsY zeolites. Unfortunately, these photooxygenations could not be carried out because there was poor loading of the substrate in these heavy-cation-exchanged Y zeolites due to the space restriction.

To acquire the size effect on the enantioselectivity for the alkyl substituent at the *C*-4 position of the oxazolidinone chiral auxiliary (*i.e.* 4-methyl *versus* 4-isopropyl), the photooxygenation of the 4-methyloxazolidinone-functionalized enecarbamates *Z*(*R*)-**2**, *Z*(*S*)-**2** or *E*(*R*)-**2**, *E*(*S*)-**2** (Fig. 2 and Scheme 1) was conducted within the MB-exchanged LiY, NaY, KY, RbY and CsY zeolites. The %ee values for the *Z*/*E* enecarbamates **2** are listed in Table 4 (Fig. 5), which reveal that in case of the 4-methyloxazolidinone-functionalized enecarbamates *Z*(*R*)-**2** or *Z*(*S*)-**2**, the maximum ee value (about 30%) was observed in KY-MB (Table 4, entry 3). In contrast, for the enecarbamates *E*(*R*)-**2** or *E*(*S*)-**2**, the maximum ee value (about 45%) was obtained in RbY-MB (Table 4, entry 4).

Analogous to the isopropyl series (Table 1), the absolute configuration of the MDB product derived from the photooxygenation of the 4-methyloxazolidinone-functionalized *E*/*Z* enecarbamates **2** depends on the alkene geometry. For example, the photooxidative cleavage of *Z*(*R*)-**2** within KY-MB afforded *S*-MDB with an ee value of 31% and the corresponding *E*(*R*)-**2** isomer gave *R*-MDB with an ee value of 17% (Table 4, entry 3). Furthermore, the enantioselectivity of the *E* and *Z* 4-methyloxazolidinone-functionalized enecarbamate **2** is considerably lower than for the corresponding *E* and *Z* isopropyl derivatives **1**. For example, the photooxygenation of the 4-methyl derivative *Z*(*R*)-**2** within NaY-MB gave the *S*-MDB with an ee value of 16% (Table 4, entry 2), whereas the 4-isopropyloxazolidinone-functionalized enecarbamate *Z*(*R*)-**1** gave *S*-MDB with an ee value of 74% (Table 1, entry 3) within NaY-MB.

## DISCUSSION

The photooxidative cleavage of 4-alkyloxazolidinone-functionalized enecarbamates to the chiral MDB product in sensitizer-exchanged MY zeolite (MY-MB) is conceptualized in form of a cartoon-like scenario in Scheme 2. The intervention of the dioxetane intermediate is reasonable, but it is a mechanistic conjecture because it has not been detected in the present work. The attractive preparative feature of such a photooxygenation is the

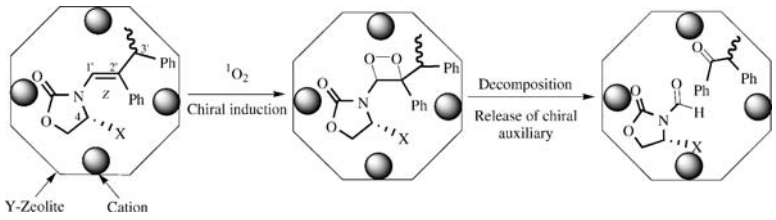


**Scheme 2.** Asymmetric induction in the photooxidative cleavage of oxazolidinone-fuctionalized enecarbamates to the chiral methyldesoxybenzoin (MDB) product within zeolite supercages.

fact that the chiral MDB product, if required, is released in the photooxidative cleavage of the alkenyl bond in the enecarbamates and may be readily separated from the oxazolidinone chiral auxiliary.

The benefit of the zeolite confinement in raising the enantioselectivity is witnessed in the %ee values for the photooxygenation of the isopropyl derivative *Z*(*S*)-**1** in the NaY-MB zeolite *versus* $CDCl_3$ in solution (Table 1; this shall be rationalized in the mechanistic model). Not only is the asymmetric induction in the zeolite much higher, but also the sense in the enantioselectivity is reversed. Namely, photooxygenation of *Z*(*S*)-**1** in the $CDCl_3$ solution the *S*-MDB product is favored, whereas in the NaY-MB zeolite it is the *R*-MDB isomer that is preferred. Evidently the spatial confinement imposed on the guest molecule within the zeolite supercages dictates profoundly the outcome of the stereoselection process (8,37,38). More than likely (6,42,43), the conformation of the enecarbamate is altered within the zeolite supercage, which influences the approach of $^1O_2$ onto the double bond of the enecarbamates to effect the observed difference in the stereoselectivity, as shall be confirmed in the mechanistic rationalization.

That the type of singlet-oxygen sensitizer does not affect the stereoselectivity is demonstrated by employing MB-exchanged *versus* thionine-exchanged NaY zeolite (25) in the photooxygenation of *Z*(*R*)-**1**. Both sensitizers gave the *S*-MDB as the major product (data not shown). Of course, no photooxidative cleavage occurs in the dark, such that $^1O_2$ is the oxidant.

Evidently, the 4-alkyl substituent in the oxazolidinone chiral auxiliary, as documented previously (35,36), is responsible for the observed enantioselectivity in the MDB product; this is substantiated in the photooxygenation of the *Z*-**3** enecarbamate. In this substrate the alkyl group at the *C*-4 position in the oxazolidinone has been replaced by a hydrogen atom and, expectedly, a racemic MDB product was obtained. Thus, the $^1O_2$ molecule attacks both $\pi$ faces of the enecarbamate double bond with equal facility and no enantioselectivity is observed. Furthermore, comparison of the enantioselectivities for the *Z* isomers (or *E* isomers) of the 4-methyl (**2**) *versus* the 4-isopropyl (**1**) enecarbamates exposes that for the latter ones the %ee values are consistently greater (see Figs. 3 and 5). Clearly, the larger 4-isopropyl group is more effective in the asymmetric induction.

A change of the configuration at the *C*-4 position of the 4-isopropyloxazolidinone chiral auxiliary in the *Z*-**1** enecarbamate from *R* to *S* results in opposite product enantiomer (*i.e*. *Z*(*R*)-**1** gave the *S*-MDB and *Z*(*S*)-**1** the *R*-MDB product in nearly the same extent of asymmetric induction [see Fig. 3]). Similar behavior was observed for the methyl derivative, except that the %ee values are significantly lower (see Fig. 5). These results demonstrate that the photooxygenation of the enecarbamates is well behaved inside the zeolites.

The effect of the *Z versus E* structural change in the photooxygenation of the enecarbamate **1** is shown in Fig. 3. Analogous to the results in solution (36), oppositely configured MDB products were also obtained in the NaY-MB zeolite: Whereas the *E*(*R*)-**1** [*E*(*S*)-**1**] favored the *R*-MDB [*S*-MDB], the *Z*(*R*)-**1** [*Z*(*S*)-**1**] isomer favored the *S*-MDB [*R*-MDB] product enantiomer in comparable %ee values, except those for the *E* isomers are consistently lower than the Z isomers (see Fig. 3). Definitely, the approach of $^1O_2$ onto the double bond of the enecarbamate is also controlled by the *E versus Z* geometry of the enecarbamates within the zeolite supercage. Similar behavior is as well observed for the methyl series, but the degree of differentiation is less pronounced (see Fig. 5).

The influence of the size of the alkali metal ion in the MY-MB zeolite was accessible only for M = Li, Na in the case of the isopropyl derivatives **1** (Tables 1 and 3) because of the poor loading of this substrate in the other alkali-metal-ion-exchanged Y-zeolites; however, a complete set of data is available for the methyl enecarbamates **2** (Table 4). Indeed, on the basis of the available X-ray structure (Turro *et al*., unpublished data) for the *E*(*S*)-**2** enecarbamate (dimension ~10.3 Å), it was anticipated that the smaller 4-methyl derivatives would fit within the supercages of all of the MY-MB (M = Li, Na, K, Cs, Rb) zeolites.

Clearly, the size of the alkali metal ion influences the extent of asymmetric induction in the photooxygenation of the 4-methyl-substituted enecarbamates **2** (Table 4). The highest but still quite modest enantioselectivity is observed for the *Z*-2 in the KY and for the *E* isomer in RbY zeolite (see Fig. 5). In contrast, for the isopropyl series it is the $Na^+$ ion (unfortunately, the remaining alkali metal ions could not be examined because they could not be loaded into the zeolite) that induces the highest enantioselectivity (Tables 1 and 3). Evidently the available free volume (6,16) in the zeolite supercage for the larger isopropyl must be more than for the smaller methyl derivative such that a smaller metal ion suffices. Presumably, this stereoselectivity behavior is a reflection of the tightness of fit of the enecarbamate within the zeolite: *The tighter the fit, the higher the asymmetric induction* (Fig. 6).

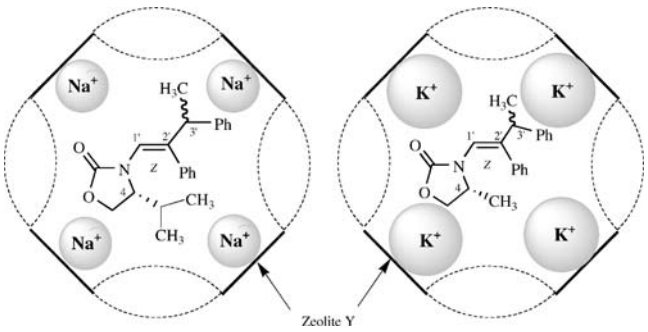


**Figure 6.** Control of the extent of asymmetric induction by the size of the metal ion in the photooxygenation of the 4-methyl- and 4-isopropyloxazolidinone enecarbamates, confined within zeolite supercage.

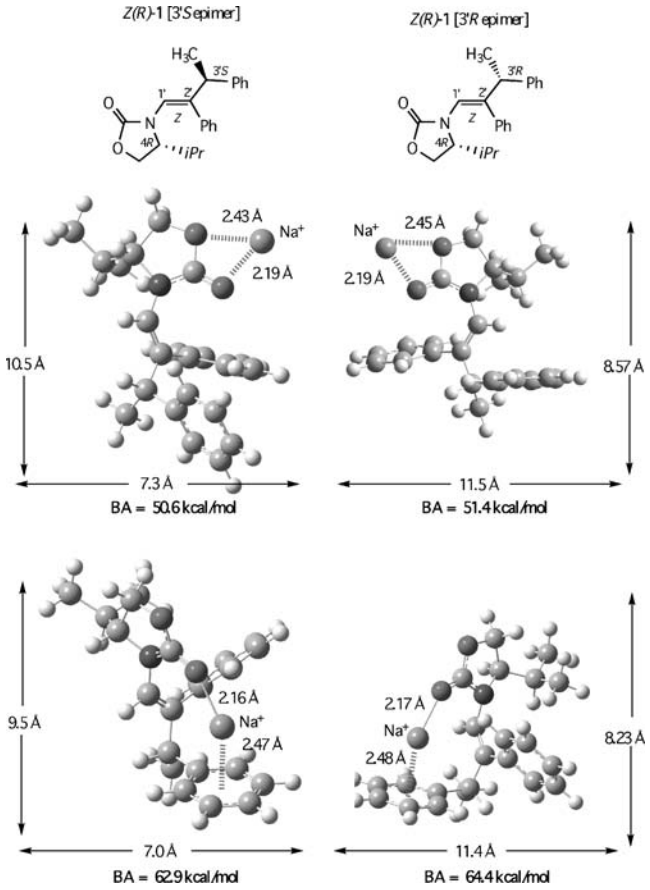


**Figure 7.** Binding affinity of $Na^+$ ions coordinated to the *Z*(*R*)-**1**-3′*S* (left) and *Z*(*R*)-**1**-3′*R* epimers (right), as computed by geometry optimization at the RB3LYP/6-31G* level.

These conspicuously complex results demand a mechanistic rationale! Fortunately, density-functional calculations (RB3LYP/6-31G* level with the Gaussian 98 program) (40) on *Z*(*R*)-**1** *viz.*, *Z*(*R*)-**1**-3′*S* and *Z*(*R*)-**1**-3′*R* epimers in Table 1 offer the mechanistic insight for understanding the role of the metal ion in the observed stereoselectivity during the photooxidative cleavage of the enecarbamates (see Fig. 7). The binding energies of the $Na^+$-bound *Z*(*R*)-**1**-3′*S* and *Z*(*R*)-**1**-3′*R* epimers show that both interact strongly with the $Na^+$ ion, with binding energies >60 kcal/mol. The simultaneous interaction of the $Na^+$ ion with the carbonyl group (dipolar interaction (44) of the oxazolidinone chiral auxiliary and the phenyl ring at the *C*-3′ position of the alkene functionality (cation-π interaction [45] afford the most stable geometry [44–51] with binding energies of 62.9 kcal/mol for the *Z*(*R*)-**1**-3′*S* and 64.4 kcal/mol for the *Z*(*R*)-**1**-3′ epimer). Such interactions reduce the conformational freedom of the enecarbamate molecule and not only ''rigidify'' it, but most likely prevent the oxidant to attack from the side of the alkene that is coordinated to the zeolite surface through the $Na^+$ ion (44–51).

The reversal of the MDB enantioselectivity in the photooxygenation of isopropyloxazolidinone-functionalized enecarbamate *Z*(*R*)-**1** in $CDCl_3$ solution (see reported [10] X-ray structure) *versus* the inside NaY zeolite (see computed structure in Fig. 7) may now be readily explained in terms of the mechanistic scenario displayed in Fig. 8. Note that in the solution case (upper structures), the oxazolidinone chiral auxiliary is essentially coplanar with the alkene functionality, whereas in the zeolite it is below the plane due to effective metal-ion coordination. For the solution case, we previously speculated (10–12,52,53) that in the attack from below the plane, the $^1O_2$ is deactivated through vibrational quenching and, thus, the more productive approach is from above to afford preferentially *R*-MDB from the *Z*-4*R*(*i*Pr)3′*R* enecarbamate epimer (the *Z*-4*R*[*i*Pr]3′*S* epimer is less reactive due to more efficient steric obstruction of the $^1O_2$ by the larger phenyl group at the *C*-3′ chirality center). For the zeolite case, we speculate that the efficient coordination of the $Na^+$ ion in the supercage wall simultaneously with the carbonyl group and the phenyl ring completely blocks out attack from below. The $^1O_2$ molecule also comes in from above, as in solution, but the stereoselection arises from the size differentiation of the hydrogen atom *versus* the methyl group at the *C*-3′ stereogenic center. Consequently, now the *S*-MDB enantiomer results in excess from the *Z*-4*R*(*i*Pr)3′*S* enecarbamate epimer. Clearly, our simple mechanistic model, which is based on the X-ray data (solution case) and computational results (zeolite case), nicely rationalizes the apparently complex stereoselectivity behavior observed in the photooxidative cleavage of the chiral enecarbamates **1** and **2**.

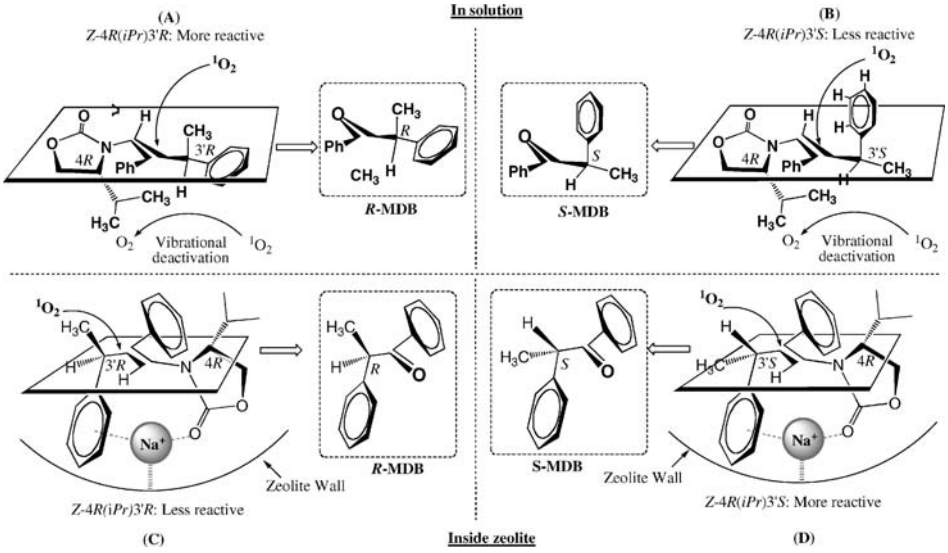


**Figure 8.** Mechanistic model for reversal of the sense in the enantioselectivity for the MDB product upon photooxidative cleavage of *Z*(*R*)-**1** in $CDCl_3$ solution (A and B) and inside NaY zeolite (C and D).

## CONCLUSION

The mechanistically rich system made up of the chiral oxazolidinone-substituted enecarbamates encaged in the dye-exchanged MY-MB zeolite, offers challenging opportunities to explore conformational, electronic, stereoelectronic and steric effects on the stereoselectivity in the photooxidative cleavage of the alkene functionality. Although the stereoselection depends on structural features such as the alkene geometry (*Z*/*E*), the size of the alkyl substituent (H, Me, *i*Pr) at the *C*-4 position in the oxazolidinone ring, the conformational preference in the epimeric enecarbamates induced by the *C*-3′ stereocenter, and the type of the metal ion (Li, Na, K, Cs, Rb) in the zeolite lattice, the salient highlight of this work is the observed anchoring of the enecarbamate substrate by the metal ion in the zeolite supercage. This confinement effect not only restricts the conformational mobility of the substrates, but also dictates the preferred attack of the oxidant in this stereoselective photooxygenation process. We are confident that such novel methodology shall prove beneficial in controlling the stereochemical outcome of other photochemical transformations.

*Acknowledgements*—The authors at Columbia thank the National Science Foundation (CHE 01-10655 and CHE-04-15516) for generous support of this research. W.A. gratefully acknowledges the financial support from the Deutsche Forschungsgemeinschaft, Alexander-von-Humboldt Stiftung, and the Fonds der Chemischen Industrie. V.R. thanks the National Science Foundation for financial support (CHE-0212042). T.P. acknowledges the support of the W.M. Keck Foundation. H.S. gratefully acknowledges a JSPS research fellowship (08384) for young scientists.

## REFERENCES

1. Turro, N. J. (2000) From boiling stones to smart crystals: supramolecular and magnetic isotope control of radical-radical reactions in zeolites. *Acc. Chem. Res.* **33**, 637–646.
2. Turro, N. J. (2002) Supramolecular organic photochemistry: control of covalent bond formation through noncovalent supramolecular interactions and magnetic effects. *Proc. Natl. Acad. Sci. USA* **99**, 4805–4809.
3. Inoue, Y. and V. Ramamurthy (2004) *Chiral Photochemistry*. Marcel Dekker, New York.
4. Inoue, Y. (1992) Asymmetric photochemical reactions in solution. *Chem. Rev.* **92**, 741–770.
5. Turro, N. J. and P. Wan (1985) Photolysis of dibenzyl ketones adsorbed on zeolite molecular sieves. Correlation of observed cage effects with carbonyl carbon-13 enrichment efficiencies. *J. Am. Chem. Soc.* **107**, 678–682.
6. Turro, N. J., C. C. Cheng, L. Abrams and D. R. Corbin (1987) Size, shape, and site selectivities in the photochemical reactions of molecules adsorbed on pentasil zeolites. Effects of coadsorbed water. *J. Am. Chem. Soc.* **109**, 2449–2456.
7. Ramamurthy, V., D. R. Corbin, N. J. Turro, Z. Zhang and M. A. Garcia Garibay (1991) Modification of photochemical reactivity by zeolites. A comparison between zeolite-solvent slurry and dry solid photolyses. *J. Org. Chem.* **56**, 255–261.
8. Sivaguru, J., A. Natarajan, L. S. Kaanumalle, J. Shailaja, S. Uppili, A. Joy and V. Ramamurthy (2003) Asymmetric photoreactions within zeolites: role of confinement and alkali metal ions. *Acc. Chem. Res.* **36**, 509–521.
9. Sivaguru, J., J. Shailaja, S. Uppili, K. Ponchot, A. Joy, N. Arunkumar and V. Ramamurthy (2002) Achieving enantio and diastereoselectivities in photoreactions through the use of a confined space. In *Organic Solid-State Reactions* (Edited by F. Toda), pp 159–188. Kluwer Academic Press, Dordrecht, the Netherlands.
10. Adam, W., S. G. Bosio and N. J. Turro (2002) Control of the mode selectivity (ene reaction versus [2 + 2] cycloaddition) in the photooxygenation of ene carbamates: directing effect of an alkenylic nitrogen functionality. *J. Am. Chem. Soc.* **124**, 14004–14005.
11. Adam, W., S. G. Bosio and N. J. Turro (2002) Highly diastereoselective dioxetane formation in the photooxygenation of enecarbamates with an oxazolidinone chiral auxiliary: steric control in the [2 + 2] cycloaddition of singlet oxygen through conformational alignment. *J. Am. Chem. Soc.* **124**, 8814–8815.
12. Adam, W., S. G. Bosio, N. J. Turro and B. T. Wolff (2004) Enecarbamates as selective substrates in oxidations: chiral-auxiliary-controlled mode selectivity and diastereoselectivity in the [2+2] cycloaddition and ene reaction of singlet oxygen and in the epioxidation by DMD and mCPBA. *J. Org. Chem.* **69**, 1704–1715.
13. Breck, D. W. (1991) *Zeolite Molecular Sieves, Chemistry and Use*. John Wiley & Sons, New York.
14. Dyer, A. (1988) *An Introduction to Zeolite Molecular Sieves*. John Wiley & Sons, New York.
15. Szostak, R. (1992) *Handbook of Molecular Sieves*. Van Nostrand Reinhold, New York.
16. Ramamurthy, V. (1991) Photoprocesses of organic molecules included in zeolites. In *Photochemistry in Organized and Confined Media* (Edited by V. Ramamurthy), Wiley-VCH, New York.
17. Grey, C. P., F. I. Poshni, A. F. Gualtieri, P. Norby, J. C. Hanson and D. R. Corbin (1997) Combined MAS NMR and X-ray powder diffraction structural characterization of hydrofluorocarbon-134 adsorbed on zeolite NaY: observation of cation migration and strong sorbate-cation interactions. *J. Am. Chem. Soc.* **119**, 1981–1989.
18. David, H. O. (1995) The crystal structure of dehydrated NaX. *Zeolites* **15**, 439–443.
19. Kirschhock, C. and H. Fuess (1996) m-Dinitrobenzene in zeolite NaY: four different arrangements. *Zeolites* **17**, 381–388.
20. Lim, K. H. and C. P. Grey (2000) Characterization of extra-framework cation positions in zeolites NaX and NaY with very fast 23Na MAS and multiple quantum MAS NMR spectroscopy. *J. Am. Chem. Soc.* **122**, 9768–9780.
21. Lim, K. H., F. Jousse, S. M. Auerbach and C. P. Grey (2001) Double resonance NMR and molecular simulations of hydrofluorocarbon binding on Faujasite zeolites NaX and NaY: the importance of hydrogen bonding in controlling adsorption geometries. *J. Phys. Chem. B.* **105**, 9918–9929.
22. Jaramillo, E., C. P. Grey and S. M. Auerbach (2001) Molecular dynamics studies of hydrofluorocarbons in Faujasite-type zeolites: modeling guest-induced cation migration in dry zeolites. *J. Phys. Chem. B.* **105**, 12319–12329.
23. Norby, P., F. I. Poshni, A. F. Gualtieri, J. C. Hanson and C. P. Grey (1998) Cation migration in zeolites: an in situ powder diffraction and MAS NMR study of the structure of zeolite Cs(Na)-Y during dehydration. *J. Phys. Chem. B.* **102**, 839–856.
24. Ramamurthy, V., D. R. Sanderson and D. F. Eaton (1993) Control of dye assembly within zeolites: role of water. *J. Am. Chem. Soc.* **115**, 10438–10439.
25. Shailaja, J., J. Sivaguru, R. J. Robbins, V. Ramamurthy, R. B. Sunoj and J. Chandrasekhar (2000) Singlet oxygen mediated oxidation of olefins within zeolites: selectivity and complexities. *Tetrahedron* **56**, 6927–6943.
26. Li, X. and V. Ramamurthy (1996) Selective oxidation of olefins within organic dye cation exchanged zeolites. *J. Am. Chem. Soc.* **118**, 10666–10667.
27. Zhou, W. and E. L. Clennan (1999) Organic reactions in zeolites. 1. Photooxidations of sulfides in methylene blue doped zeolite Y. *J. Am. Chem. Soc.* **121**, 2915–2916.
28. Clennan, E. L. and J. P. Sram (2000) Photochemical reactions in the interior of a zeolite. Part 5: the origin of the zeolite induced regioselectivity in the singlet oxygen ene reaction. *Tetrahedron* **56**, 6945–6950.
29. Stratakis, M., D. Kalaitzakis, D. Stavroulakis, G. Kosmas and C. Tsangarakis (2003) Remarkable change of the diastereoselection in the dye-sensitized ene hydroperoxidation of chiral alkenes by zeolite confinement. *Org. Lett.* **5**, 3471–3474.
30. Stratakis, M. and G. Froudakis (2000) Site specificity in the photooxidation of some trisubstituted alkenes in thionin-supported zeolite Na-Y. On the role of the alkali metal cation. *Org. Lett.* **2**, 1369–1372.
31. Foote, C. S. (1968) Photosensitized oxygenations and the role of singlet oxygen. *Acc. Chem. Res.* **1**, 104–110.
32. Frimer, A. A. (1965) *Singlet Oxygen Part I–IV*. Boca Raton, FL.
33. Gollnick, K. and H. J. Kuhn (1979) Ene-reactions with singlet oxygen. In *Singlet Oxygen* (Edited by H. H. Wasserman and R. W. Murray), pp. 287–427. Academic Press, New York.

34. Wasserman, H. H. and R. W. Murray (1979) *Singlet Oxygen*. Academic Press, New York.
35. Sivaguru, J., T. Poon, R. Franz, S. Jockusch, W. Adam and N. J. Turro (2004) Stereocontrol within confined spaces: enantioselective photooxidation of enecarbamates inside zeolite supercages. *J. Am. Chem. Soc.* **126**, 10816–10817.
36. Poon, T., J. Sivaguru, R. Franz, S. Jockusch, C. Martinez, I. Washington, W. Adam, Y. Inoue and N. J. Turro (2004) Temperature and solvent control of the stereoselectivity in the reactions of singlet oxygen with oxazolidinone-substituted enecarbamates. *J. Am. Chem. Soc.* **126**, 10498–10499.
37. Sivaguru, J., R. B. Sunoj, T. Wada, Y. Origane, Y. Inoue and V. Ramamurthy (2004) Enhanced eiastereoselectivity via confinement: photoisomerization of 2,3-diphenylcyclopropane-1-carboxylic acid derivatives within zeolites. *J. Org. Chem.* **69**, 6533–6547.
38. Sivaguru, J., R. B. Sunoj, T. Wada, Y. Origane, Y. Inoue and V. Ramamurthy (2004) Enhanced diastereoselectivity via confinement: diastereoselective photoisomerization of 2,3-diphenyl-1-benzoylcyclopropane derivatives within zeolites. *J. Org. Chem.* **69**, 5528–5536.
39. Jockusch, S., J. Sivaguru, N. J. Turro and V. Ramamurthy (2005) Direct measurement of the singlet oxygen lifetime in zeolites by near-IR phosphorescence. *Photochem. Photobiol. Sci.* **4**, 403–405.
40. Frisch, M. J., G. W. Trucks, H. B. Schlegel, G. E. Scuseria, M. A. Robb, J. R. Cheeseman, J. J. A. Montgomery, T. K. Vreven, K. N., J. C. Burant, J. M. Millam, S. S. Iyengar, J. Tomasi, V. Barone, B. Mennucci, M. Cossi, G. Scalmani, N. Rega, G. A. Petersson, H. Nakatsuji, M. Hada, M. Ehara, K. Toyota, R. Fukuda, J. Hasegawa, M. Ishida, T. Nakajima, Y. Honda, O. Kitao, H. Nakai, M. Klene, X. Li, J. E. Knox, H. P. Hratchian, J. B. Cross, V. Bakken, C. Adamo, J. Jaramillo, R. Gomperts, R. E. Stratmann, O. Yazyev, A. J. Austin, R. Cammi, C. Pomelli, J. W. Ochterski, P. Y. Ayala, K. Morokuma, G. A. Voth, P. Salvador, J. J. Dannenberg, V. G. Zakrzewski, S. Dapprich, A. D. Daniels, M. C. Strain, O. Farkas, D. K. Malick, A. D. Rabuck, K. Raghavachari, J. B. Foresman, J. V. Ortiz, Q. Cui, A. G. Baboul, S. Clifford, J. Cioslowski, B. B. Stefanov, G. Liu, A. Liashenko, P. Piskorz, I. Komaromi, R. L. Martin, D. J. Fox, T. Keith, M. A. Al-Laham, C. Y. Peng, A. Nanayakkara, M. Challacombe, P. M. W. Gill, B. Johnson, W. Chen, M. W. Wong, C. Gonzalez and J. A. Pople (1998) *Gaussian 98, Revision A.11*; Gaussian, Inc., Pittsburgh, PA.
41. Poon, T., J. Turro Nicholas, J. Chapman, P. Lakshminarasimhan, X. Lei, W. Adam and G. Bosio Sara (2003) A supramolecular ''ship in bottle'' strategy for enantiomeric selectivity in geminate radical pair recombination. *Org. Lett.* **5**, 2025–2028.
42. Ramamurthy, V., D. R. Corbin, D. F. Eaton and N. J. Turro (1989) Modification of photochemical reactivity by zeolites: role of cations in controlling the behavior of radicals generated within faujasites. *Tetrahedron Lett.* **30**, 5833–5836.
43. Ramamurthy, V., D. R. Corbin, N. J. Turro and Y. Sato (1989) Modification of photochemical reactivity by zeolites: cation enhanced a-cleavage of aryl alkyl ketones included in faujasites. *Tetrahedron Lett.* **30**, 5829–5832.
44. Raber, D. J., N. K. Raber, J. Chandrasekhar and P. v. R. Schleyer (1984) Geometries and energies of complexes between formaldehyde and first- and second-row cations. A theoretical study. *Inorg. Chem.* **23**, 4076–4080.
45. Ma, J. C. and D. A. Dougherty (1997) The cation-π interaction. *Chem. Rev.* **97**, 1303–1324.
46. Dunbar, R. C. (2000) Complexation of Na+ and K+ to aromatic amino acids: a density functional computational study of cation-π interactions. *J. Phys. Chem. A* **104**, 8067–8074.
47. Hoyau, S. and G. Ohanessian (1998) Interaction of alkali metal cations (Li+-Cs+) with glycine in the gas phase: a theoretical study. *Chem. Eur. J.* **4**, 1561–1569.
48. Jockusch, R. A., A. S. Lemoff and E. R. William (2001) Effect of metal ion and water coordination on the structure of a gas-phase amino acid. *J. Am. Chem. Soc.* **123**, 12255–12265.
49. Jockusch, R. A., W. D. Price and E. R. Williams (1999) Structure of cationized arginine (Arg • M+, M = H, Li, Na, K, Rb, and Cs) in the gas phase: further evidence for zwitterionic arginine. *J. Phys. Chem. A* **103**, 9266–9274.
50. Siu, F. M., N. L. Ma and C. W. Tsang (2001) Cation-π interactions in sodiated phenylalanine complexes: is phenylalanine in the charge-solvated or zwitterionic form? *J. Am. Chem. Soc.* **123**, 3397–3398.
51. Wyttenbach, T., M. Witt and M. T. Bowers (2000) On the stability of amino acid zwitterions in the gas phase: the influence of derivatization, proton affinity, and alkali ion addition. *J. Am. Chem. Soc.* **122**, 3458–3464.
52. Poon, T., N. J. Turro, J. Chapman, P. Lakshminarasimhan, X. Lei, S. Jockusch, R. Franz, I. Washington, W. Adam and S. G. Bosio (2003) Stereochemical features of the physical and chemical interactions of singlet oxygen with enecarbamates. *Org. Lett.* **5**, 4951–4953.
53. Sivaguru, J., H. Saito, T. Poon, T. Omonuwa, R. Franz, S. Jockusch, C. Hooper, Y. Inoue, W. Adam and N. J. Turro (2005) Stereoselective photooxidation of enecarbamates: reactivity of ozone vs singlet oxygen. *Org. Lett.* **7**, 2089–2092.